Cell Reports, Volume *16*

Supplemental Information

A Functional Link between AMPK and Orexin Mediates the Effect of BMP8B on Energy Balance

Luís Martins, Patricia Seoane-Collazo, Cristina Contreras, Ismael González-García, Noelia Martínez-Sánchez, Francisco González, Juan Zalvide, Rosalía Gallego, Carlos Diéguez, Rubén Nogueiras, Manuel Tena-Sempere, and Miguel López

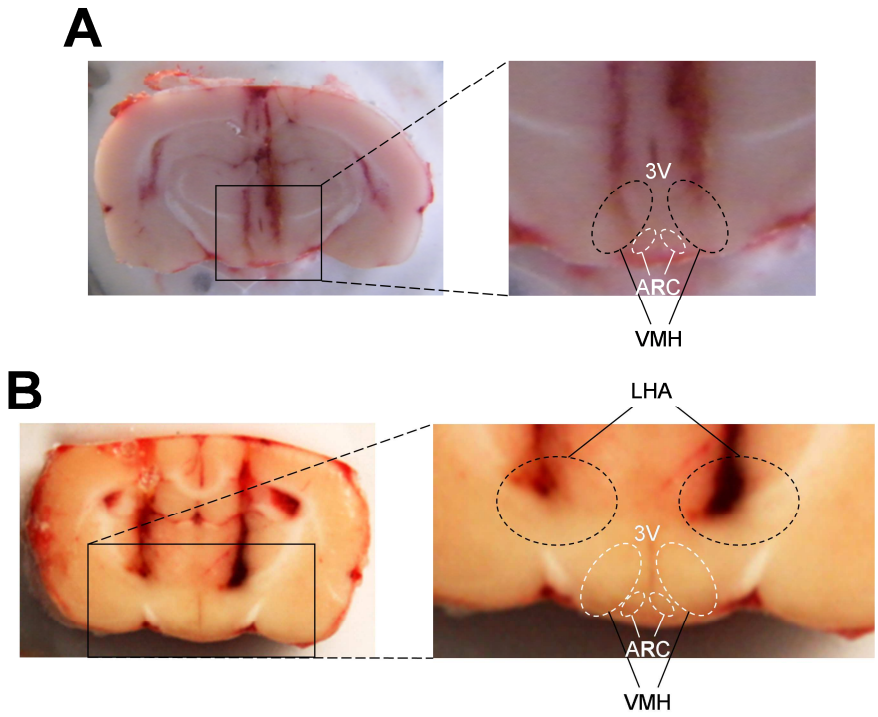

FIGURE S1 related to Figure 2. Anatomical validation of VMH and LHA injections
Coronal sections of rat brains showing the localization of the cannulae in the VMH **(A)** and the LHA **(B).**

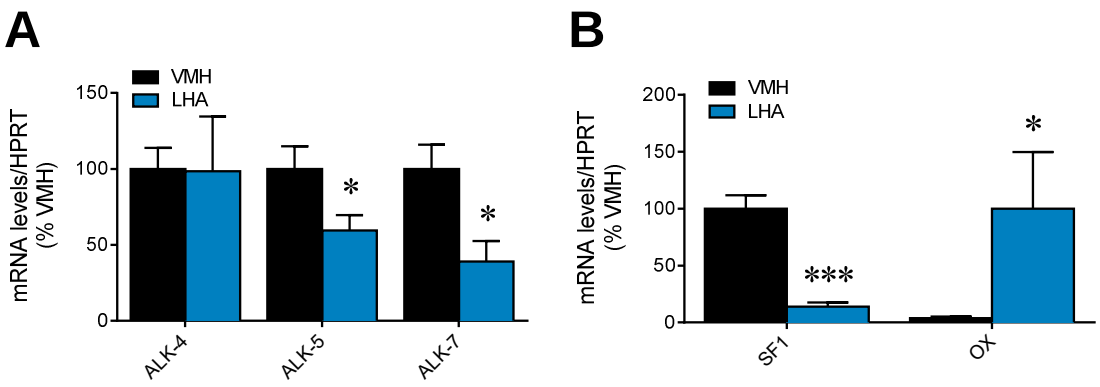

FIGURE S2 related to Figure 2. Hypothalamic expression of BMP8B Type I receptors
(A) mRNA expression of BMP8B Type I receptors . Data are expressed as mean ± SEM; n=4-6 animals per experimental group. * and *** P<0.01 and 0.001 *vs.* VMH, # P<0.05 *vs.* LHA.

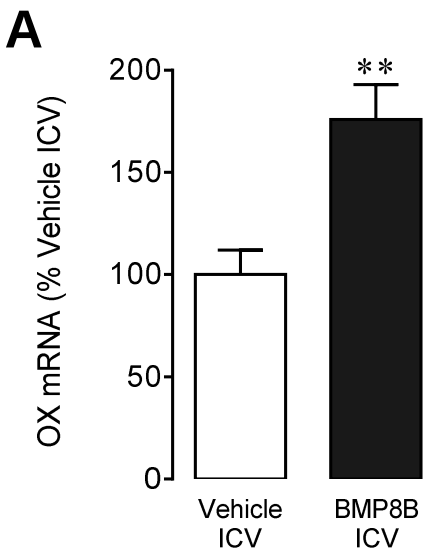

FIGURE S3 related to Figure 4. Effect of central administration of BMP8B on OX in the LHA

(A) OX mRNA levels in the LHA of rats receiving ICV administration of vehicle of BMP8B. Data are expressed as mean ± SEM; n=8 animals per experimental group. ** P<0.01 *vs.* vehicle

Table S1 related to Figures 3 and S2: Primers and probes for real-time PCR (TaqMan®) analysis

mRNA	GenBank Accession Number		Sequence
ALK-4	NM_199230.1	Assay ID	ThermoFisher TaqMan® Gene Expression Assays Assay ID Rn01761726_m1
ALK-5	NM_012775.2	Assay ID	ThermoFisher TaqMan® Gene Expression Assays Assay ID Rn00688966_m1
ALK-7	NM_139090.1	Assay ID	ThermoFisher TaqMan® Gene Expression Assays Assay ID Rn00594657_m1
CIDEA	NM_001170467.1	Assay ID	ThermoFisher TaqMan® Gene Expression Assays Assay ID Rn04181355_m1
FABP3	NM_024162.1	Fw Primer Rv Primer Probe	5'-ACGGAGGCAAACTGGTCCAT-3' 5'-CACTTAGTTCCCGTGTAAGCGTAGTC-3' FAM-5'-TGCAGAAGTGGGACGGGCAGG-3'-TAMRA
HPRT	NM_012583	Fw Primer Rv Primer Probe	5'-AGCCGACCGGTTCTGTCAT-3' 5'-GGTCATAACCTGGTTCATCATCAC -3' FAM-5'- CGACCCTCAGTCCCAGCGTCGTGAT 3'-TAMRA
PGC1α	NM_031347	Fw Primer Rv Primer Probe	5'-CGATCACCATATTCCAGGTCAAG-3' 5'-CGATGTGTGCGGTGTCTGTAGT -3' 5'-AGGTCCCCAGGCAGTAGATCCTCTTCAAGA -3'
PGC1β	NM_176075	Assay ID	ThermoFisher TaqMan® Gene Expression Assays Assay ID Rn00598552_m1
PRDM16	XM_008764418.1	Assay ID	ThermoFisher TaqMan® Gene Expression Assays Assay ID Mm01266512_m1
UCP1	NM_012682	Fw Primer Rv Primer Probe	5'-CAATGACCATGTACACCAAGGAA-3' 5'-GATCCGAGTCGCAGAAAAGAA-3' FAM-5'-ACCGGCAGCCTTTTTCAAAGGGTTTG-3'-TAMRA
UCP3	NM_003356.3	Assay ID	ThermoFisher TaqMan® Gene Expression Assays Assay ID Rn00565874_m1

SUPPLEMENTAL EXPERIMENTAL PROCEDURES

Ovariectomy and estradiol replacement

Sprague-Dawley rats were bilaterally ovariectomized (OVX) or sham-operated as described previously (Martínez de Morentin et al., 2014; Martinez de Morentin et al., 2015). Estradiol treatment was carried out three weeks after surgery to ensure a total washout of endogenous ovarian hormones. OVX rats received a daily SC injection of estradiol (estradiol benzoate; 2 µg dissolved in 100 µL of sesame oil; both from *Sigma;* St Louis, MO, USA) or vehicle (100 µL of sesame oil; control rats) during 3 days (Martínez de Morentin et al., 2014; Martinez de Morentin et al., 2015).

Intracerebroventricular and nucleus-specific treatments

ICV cannulae were implanted under ketamine/xylazine anesthesia, as previously described (Nogueiras et al., 2007; López et al., 2008; López et al., 2010; Whittle et al., 2012; Martínez de Morentin et al., 2012; Imbernon et al., 2013; Martínez de Morentin et al., 2014; Contreras et al., 2014; Beiroa et al., 2014). Animals were individually caged and allowed to recover for four days. For BMP8B acute experiments, animals were ICV treated with vehicle (5 µL of saline for rats and 2 µL of saline for mice) or BMP8B (5 µL of 4nM BMP8B for rats and 2 µL of 100 pM BMP8B for mice) (*R&D Systems*, Minneapolis, MN, USA); animals were treated at 09:00 AM (one hour after the light cycle had commenced). For the cold exposure experiments female rats (experiments were repeated twice and the number of animals per experimental group was 4-8 in each replicate, a representative experiment is shown) or mice (the number of animals per experimental group was 6-8) were housed in a climate chamber at 4ºC. BMP8B was

ICV administered (at the above dose) after 10 hours and maintained the animals in a cold environment for a total 12 hours.

For the experiment with the selective orexin 1 receptor (OX1R) antagonist, rats received an ICV injection of vehicle (5 μL of DMSO; *Sigma*; St Louis, MO, USA) or SB-334867 (10 nmol in 5μL; *Tocris Bioscience*; Bristol, UK) (Jia et al., 2012) 30 minutes prior to BMP8B administration. The experiments were repeated five times and the number of animals per experimental group was 6-8 in each of replicate (total number of animals of 30-40 per experimental group).

For chronic treatments, BMP8B (0.1 pmol/day/rat) was delivered via a permanent 28-gauge stainless steel cannula (*Plastics One*, Roanoke, VA, USA) inserted bilaterally either in VMH or LHA, directed to the following stereotaxic coordinates: 2.8 mm posterior to bregma, ±0.6 mm lateral to midline and 10.1 mm ventral or 2.9 mm posterior to bregma, ±2.0 mm lateral to midline and 8.1 mm ventral, respectively (Imbernon et al., 2013; Contreras et al., 2014). A catheter tube was connected from each infusion cannula to an osmotic minipump flow moderator (Model 1007D; *Alzet Osmotic Pumps*, Cupertino, CA, USA). These pumps had a flow rate of 0,5 μL/hour during 7 days of treatment. The osmotic minipumps were inserted in a subcutaneous pocket on the dorsal surface created using blunt dissection and the treatment was given during 7 days. The experiments were repeated twice and the number of animals per experimental group was 8 in each of replicate (total number of 16 animals per experimental group).

Stereotaxic microinjection of adenoviral and lentiviral vectors

Rats were placed in a stereotaxic frame (*David Kopf Instruments;* Tujunga, CA, USA) under ketamine-xylazine anesthesia. The VMH was targeted bilaterally using a 25-gauge needle (*Hamilton;* Reno, NV, USA). The injections were directed to the

following stereotaxic coordinates for the VMH: 2.4/3.2 mm posterior to the bregma (two injections were performed in each VMH), ±0.6 mm lateral to midline and 10.1 mm ventral as previously reported (López et al., 2008; López et al., 2010; Whittle et al., 2012; Martínez de Morentin et al., 2012; Martínez de Morentin et al., 2014; Contreras et al., 2014; Beiroa et al., 2014). Adenoviral vectors (*Viraquest;* North Liberty, IA, USA) containing green fluorescence protein (GFP, used as control) or a constitutive active isoform of AMPKα (AMPKα-CA) (wild-type, at 10^{12} pfu/ml) were delivered at a rate of 200 nl/min for 5 min (1 µl/injection site) as previously reported (López et al., 2008; López et al., 2010; Whittle et al., 2012; Martínez de Morentin et al., 2012; Martínez de Morentin et al., 2014; Contreras et al., 2014; Beiroa et al., 2014). Animals were treated with BMP8B during 2 hours. The experiment was repeated twice and the number of animals per experimental group was 6 in each replicate (total number of 12 animals per experimental group).

Lentiviral vectors (*Sigma;* St. Louis, MO, USA) containing green fluorescence protein (TurboGFP (SHC003V, used as control) or a shRNA targeting VGLUT2 (at 10^6 TU/ml) were delivered at the LHA (2.9 mm posterior to bregma, ±2.0 mm lateral to midline and 8.1 mm ventral). Animals were treated 28 days prior to BMP8B ICV treatment that lasted 2 hours. The number of animals per experimental group was 9.

Energy expenditure, locomotor activity, respiratory quotient and nuclear magnetic resonance analysis

Rats were analyzed for EE, RQ and LA using a calorimetric system (*LabMaster; TSE Systems;* Bad Homburg, Germany), as previously shown (Nogueiras et al., 2007; Martínez de Morentin et al., 2012; Imbernon et al., 2013; Martínez de Morentin et al., 2014). Rats were placed for adaptation for 1 week before starting the measurements. For

the measurement of body composition, we used NMR imaging (*Whole Body Composition Analyzer; EchoMRI;* Houston, TX), as previously shown (Martínez de Morentin et al., 2012; Imbernon et al., 2013; Martínez de Morentin et al., 2014). We used 8 animals per experimental group.

Temperature measurements

Body temperature was recorded twice at the beginning and the end of the treatments with a rectal probe connected to digital thermometer (*BAT-12 Microprobe-Thermometer; Physitemp*; NJ, USA). Skin temperature surrounding BAT was recorded with an infrared camera (*B335 Thermal Imaging Camera; FLIR*; West Malling, Kent, UK) (Whittle et al., 2012; Martínez de Morentin et al., 2012; Martínez de Morentin et al., 2014; Contreras et al., 2014; Beiroa et al., 2014).

Sample processing

Rats and mice were killed by cervical dislocation. From each animal, either the whole brain (for *in situ* hybridization) or the VMH and LHA (dissected from the whole hypothalamus for RT-PCR or western blot), as well as the BAT (for western blot) were harvested and immediately homogenized on ice to preserve phosphorylated protein levels. Samples were stored at -80ºC until further processing. Dissection of the VMH and LHA was performed by micropunches under the microscope, as previously shown (López et al., 2010; Whittle et al., 2012; Martínez de Morentin et al., 2014; Contreras et al., 2014; Beiroa et al., 2014). The specificity of the VMH and LHA dissections was confirmed by analyzing the mRNA of steroidogenic factor-1 and prepro- orexin **(Figure S2B).**

In situ hybridization

Coronal brain sections (16 μm) were probed with a specific oligonucleotide for prepro-OX (*GenBank Accession Number*: NM_013179; 5'-TTC GTA GAG ACG GCA GGA ACA CGT CTT CTG GCG ACA-3') as previously published (López et al., 2008; López et al., 2010; Whittle et al., 2012; Martínez de Morentin et al., 2012; Álvarez-Crespo et al., 2013; Martínez de Morentin et al., 2014). Sections were scanned and the hybridization signal was quantified by densitometry using *ImageJ-1.33* software (*NIH*, Bethesda, MD, USA). We used 6-8 animals per experimental group and 16-20 sections for each animal (4-5 slides with four sections per slide). The mean of these 16-20 values was used as densitometry value for each animal.

Western Blotting

VMH, LHA and BAT protein lysates were subjected to SDS-PAGE, electrotransferred on a PVDF membrane and probed with the following antibodies: AMPKα1, AMPKα2 (Millipore, Billerica, MA, USA); FAS (*BD*; Franklin Lakes, NJ, USA), ACC, pACC-Ser^{79}, pAMPK-Thr^{172} (*Cell Signaling;* Danvers; MA, USA); α-tubulin, β-actin (*Sigma;* St. Louis, MO, USA); VGLUT2 and UCP1 (*Abcam*; Cambridge, UK) as previously described (López et al., 2008; López et al., 2010; Whittle et al., 2012; Martínez de Morentin et al., 2012; Martínez de Morentin et al., 2014; Contreras et al., 2014; Beiroa et al., 2014). Values were expressed in relation to α-tubulin (for BAT) or β-actin (for VMH and LHA) protein levels. We used 4-8 animals per experimental group.

Real-time PCR

We perform real-time PCR (*TaqMan®*; *Applied Biosystems*; Carlsbad, CA, USA) as previously described (López et al., 2010; Whittle et al., 2012; Martínez de Morentin et al., 2012; Martínez de Morentin et al., 2014) using specific sets of primers and probes **(Table S1)**. Values were expressed relative to Hypoxanthine-guanine phosphoribosyltransferase (HPRT) levels. We used 8-9 animals per experimental group.

Immunohistochemistry

Detection of UCP1 in WAT was performed using anti-UCP1 (1:500; *Abcam*, Cambridge, UK). Detection was done with an anti-rabbit antibody conjugated with Alexa 488 (1:200; *Molecular Probes*; Grand Island, NY, US) as previously reported (Folgueira et al., 2016). Detection of GFP was performed with an immunofluorescence procedure, using a rabbit anti-GFP (1:200; *Abcam*; Cambridge, UK). Detection was done with an anti-rabbit antibody conjugated with *Alexa 488* (1:200; *Molecular Probes;* Grand Island, NY, US) as previously reported (López et al., 2008; López et al., 2010; Varela et al., 2012; Whittle et al., 2012; Imbernon et al., 2013). Images were taken with a digital camera *Olympus XC50* (*Olympus Corporation*, Tokyo, Japan) at 20X. Digital images were quantified with ImageJ Software (*National Institutes of Health*, USA).

SUPPLEMENTAL REFERENCES

Álvarez-Crespo,M., Martinez-Sanchez,N., Ruiz-Pino,F., Garcia-Lavandeira,M., Alvarez,C.V., Tena-Sempere,M., Nogueiras,R., Diéguez,C., and López,M. (2013). The orexigenic effect of orexin-A revisited: dependence of an intact growth hormone axis. Endocrinology *154*, 3589-3598.

Beiroa,D., Imbernon,M., Gallego,R., Senra,A., Herranz,D., Villaroya,F., Serrano,M., Ferno,J., Salvador,J., Escalada,J., Dieguez,C., Lopez,M., Fruhbeck,G., and Nogueiras,R. (2014). GLP-1 Agonism Stimulates Brown Adipose Tissue Thermogenesis and Browning Through Hypothalamic AMPK. Diabetes *63*, 3346-3358.

Contreras,C., González-García,I., Martínez-Sánchez,N., Seoane-Collazo,P., Jacas,J., Morgan,D.A., Serra,D., Gallego,R., González,F., Casals,N., Nogueiras,R., Rahmouni,K., Diéguez,C., and López,M. (2014). Central Ceramide-Induced Hypothalamic Lipotoxicity and ER Stress Regulate Energy Balance. Cell Rep. *9*, 366-377.

Folgueira,C., Beiroa,D., Callon,A., Al-Massadi,O., Barja-Fernandez,S., Senra,A., Ferno,J., Lopez,M., Dieguez,C., Casanueva,F.F., Rohner-Jeanrenaud,F., Seoane,L.M., and Nogueiras,R. (2016). Uroguanylin Action in the Brain Reduces Weight Gain in Obese Mice via Different Efferent Autonomic Pathways. Diabetes *65*, 421-432.

Imbernon,M., Beiroa,D., Vazquez,M.J., Morgan,D.A., Veyrat-Durebex,C., Porteiro,B., Diaz-Arteaga,A., Senra,A., Busquets,S., Velasquez,D.A., Al-Massadi,O., Varela,L., Gandara,M., Lopez-Soriano,F.J., Gallego,R., Seoane,L.M., Argiles,J.M., López,M., Davis,R.J., Sabio,G., Rohner-Jeanrenaud,F., Rahmouni,K., Diéguez,C., and Nogueiras,R. (2013). Central Melanin-Concentrating Hormone Influences Liver and Adipose Metabolism Via Specific Hypothalamic Nuclei and Efferent Autonomic/JNK1 Pathways. Gastroenterology *144*, 636-649.

Jia,X., Yan,J., Xia,J., Xiong,J., Wang,T., Chen,Y., Qi,A., Yang,N., Fan,S., Ye,J., and Hu,Z. (2012). Arousal effects of orexin A on acute alcohol intoxication-induced coma in rats. Neuropharmacology *62*, 775-783.

López,M., Lage,R., Saha,A.K., Pérez-Tilve,D., Vázquez,M.J., Varela,L., Sangiao-Alvarellos,S., Tovar,S., Raghay,K., Rodríguez-Cuenca,S., Deoliveira,R.M., Castañeda,T., Datta,R., Dong,J.Z., Culler,M., Sleeman,M.W., Álvarez,C.V., Gallego,R., Lelliott,C.J., Carling,D., Tschop,M.H., Diéguez,C., and Vidal-Puig,A. (2008). Hypothalamic fatty acid metabolism mediates the orexigenic action of ghrelin. Cell Metab *7*, 389-399.

López,M., Varela,L., Vázquez,M.J., Rodríguez-Cuenca,S., González,C.R., Velagapudi,V.R., Morgan,D.A., Schoenmakers,E., Agassandian,K., Lage,R., de Morentin,P.B., Tovar,S., Nogueiras,R., Carling,D., Lelliott,C., Gallego,R., Oresic,M., Chatterjee,K., Saha,A.K., Rahmouni,K., Diéguez,C., and Vidal-Puig,A. (2010). Hypothalamic AMPK and fatty acid metabolism mediate thyroid regulation of energy balance. Nat. Med. *16*, 1001-1008.

Martínez de Morentin,P.B., Gónzalez-García,I., Martins,L., Lage,R., Fernández-Mallo,D., Martínez-Sánchez,N., Ruíz-Pino,F., Liu,J., Morgan,D.A., Pinilla,L., Gallego,R., Saha,A.K., Kalsbeek,A., Fliers,E., Bisschop,P.H., Diéguez,C., Nogueiras,R., Rahmouni,K., Tena-Sempere,M., and López,M. (2014). Estradiol regulates brown adipose tissue thermogenesis via hypothalamic AMPK. Cell Metab *20*, 41-53.

Martinez de Morentin,P.B., Lage,R., Gonzalez-Garcia,I., Ruiz-Pino,F., Martins,L., Fernandez-Mallo,D., Gallego,R., Ferno,J., Senaris,R., Saha,A.K., Tovar,S., Dieguez,C., Nogueiras,R., Tena-Sempere,M., and Lopez,M. (2015). Pregnancy induces resistance to the anorectic effect of hypothalamic malonyl-CoA and the thermogenic effect of hypothalamic AMPK inhibition in female rats. Endocrinology *156*, 947-960.

Martínez de Morentin,P.B., Whittle,A.J., Ferno,J., Nogueiras,R., Diéguez C, Vidal-Puig,A., and López M (2012). Nicotine induces negative energy balance through hypothalamic AMP-activated protein kinase. Diabetes *61*, 807-817.

Nogueiras,R., Wiedmer,P., Perez-Tilve,D., Veyrat-Durebex,C., Keogh,J.M., Sutton,G.M., Pfluger,P.T., Castaneda,T.R., Neschen,S., Hofmann,S.M., Howles,P.N., Morgan,D.A., Benoit,S.C., Szanto,I.,

Schrott,B., Schurmann,A., Joost,H.G., Hammond,C., Hui,D.Y., Woods,S.C., Rahmouni,K., Butler,A.A., Farooqi,I.S., O'rahilly,S., Rohner-Jeanrenaud,F., and Tschop,M.H. (2007). The central melanocortin system directly controls peripheral lipid metabolism. J. Clin. Invest *117*, 3475-3488.

Varela,L., Martínez-Sánchez N., Gallego,R., Vázquez,M.J., Roa,J., Gándara M., Schoenmakers,E., Nogueiras,R., Chatterjee,K., Tena-Sempere,M., Diéguez C, and López M (2012). Hypothalamic mTOR pathway mediates thyroid hormone-induced hyperphagia in hyperthyroidism. J. Pathol. *227*, 209-222.

Whittle,A.J., Carobbio S, Martíns L, Slawik,M., Hondares,E., Vázquez,M.J., Morgan D, Csikasz, RI, Gallego,R., Rodriguez-Cuenca,S., Dale,M., Virtue,S., Villarroya,F., Cannon,B., Rahmouni,K., López M, and Vidal-Puig,A. (2012). Bmp8b increases brown adipose tissue thermogenesis through both central and peripheral actions. Cell *149*, 871-885.